



Article

Effects of the Construction of Granadilla Industrial Port in Seagrass and Seaweed Habitats Using Very-High-Resolution Multispectral Satellite Imagery

Antonio Mederos-Barrera ^{1,*} , José Sevilla ², Javier Marcello ¹ , José María Espinosa ² and Francisco Eugenio ¹

¹ Instituto de Oceanografía y Cambio Global, Universidad de Las Palmas de Gran Canaria, Unidad Asociada ULPGC-CSIC, Campus Universitario de Tafira, 35017 Las Palmas de Gran Canaria, Spain

² Fundación del Sector Público Estatal Observatorio Ambiental Granadilla, Vía Interior del Puerto de Santa Cruz de Tenerife, Edificio Puerto-Ciudad, 38001 Santa Cruz de Tenerife, Spain

* Correspondence: mederosbarrera.antonio@gmail.com

Abstract: Seagrass and seaweed meadows hold a very important role in coastal and marine ecosystems. However, anthropogenic impacts pose risks to these delicate habitats. This paper analyses the multitemporal impact of the construction of the largest industrial port in the Canary Islands, near the Special Area of Conservation Natura 2000, on *Cymodocea nodosa* seagrass meadows (sebadales) of the South of Tenerife, in the locality of Granadilla (Canary Islands, Spain). Very-high-resolution WorldView-2 multispectral satellite data were used for the analysis. Specifically, three images were selected before, during, and after the construction of the port (2011, 2014, and 2022, correspondingly). Initially, advanced pre-processing of the images was performed, and then seabed maps were obtained using the machine learning K-Nearest Neighbors (KNN) supervised classification model, discriminating 12 different bottom types in Case-2 complex waters. The maps achieved high-quality metrics with Precision values of 85%, 81%, and 80%, recall of 76%, 77%, and 77%, and F₁ scores of 80%, 79%, and 77% for 2011, 2014, and 2022, respectively. The results mainly show that the construction directly affected the seagrass and seaweed habitats. In particular, the impact of the port on the meadows of *Cymodocea nodosa*, *Caulerpa prolifera*, and *maërl* was assessed. The total *maërl* population was reduced by 1.9 km² throughout the study area. However, the *Cymodocea nodosa* population was maintained at the cost of colonizing *maërl* areas. Furthermore, the port sedimented a total of 0.98 km² of seabed, especially *Cymodocea nodosa* and *maërl*. In addition, it was observed that *Caulerpa prolifera* was established as a meadow at the entrance of the port, replacing part of the *Cymodocea nodosa* and *maërl* areas. As additional results, bathymetric maps were generated from satellite imagery with the Sigmoid model, and the presence of a submarine outfall was, as well, presented.

Keywords: industrial port; assessment impact; satellite imagery; benthic maps; bathymetry maps; WorldView-2



Citation: Mederos-Barrera, A.; Sevilla, J.; Marcello, J.; Espinosa, J.M.; Eugenio, F. Effects of the Construction of Granadilla Industrial Port in Seagrass and Seaweed Habitats Using Very-High-Resolution Multispectral Satellite Imagery. *Remote Sens.* **2024**, *16*, 945. <https://doi.org/10.3390/rs16060945>

Academic Editor: SeungHyun Son

Received: 15 January 2024

Revised: 29 February 2024

Accepted: 5 March 2024

Published: 8 March 2024



Copyright: © 2024 by the authors. Licensee MDPI, Basel, Switzerland. This article is an open access article distributed under the terms and conditions of the Creative Commons Attribution (CC BY) license (<https://creativecommons.org/licenses/by/4.0/>).

1. Introduction

Seagrass meadows constitute a critical role in coastal and marine ecosystems [1,2]. The benefits can be grouped into the following categories [3]: coastal protection against erosion, improved water quality, habitats development for a diversity of marine species, and a large carbon sink absorbing up to 12% of the carbon absorbed by oceans [4]. However, anthropogenic activity has a significant impact on seagrass meadows globally, where an annual loss of 2% to 5% can be reported [5,6]. However, the loss of seagrass meadows is not linear, and between the 1990s and 2000s, the population did not appear to be declining as fast, although it was still decreasing [7]. In the case of eastern North Atlantic waters, it is estimated that 70% of seagrass has been lost since the initial surveys were conducted [7]. Some commercial activities that influence seagrass meadows loss can be coastal construction (such as ports), agricultural waste, or industrial discharges such as

from desalination plants [8]. On the other hand, regarding indirect impact, it should be noted that climate change produces different effects, such as an increase in temperature that produces changes in distribution and growth, as well as changes in carbon balance. Other effects are alterations in the availability of photosynthetically active radiation (PAR) from visible light and ultraviolet radiation, or increases in storm intensity and possibly frequency, increasing sediment deposition [9,10]. Finally, flooding, that produces sedimentation and reduces irradiance, or sea level rises and alterations in currents, that also produce a decrease in available radiation and increased turbidity, can be expected [11].

Furthermore, it is worth mentioning the great importance of seaweed meadows, which have a multitude of benefits for marine and coastal ecosystems [12,13]. Seaweed meadows also provide a specific habitat area for some species, improve water quality, provide coastal protection elements, and allow carbon sequestration, mitigating the effects of climate change. In turn, like seagrass, seaweed meadows are endangered by human impact [14]. As can be seen, there are many similarities between the benefits and risks of seagrass and seaweed meadows. However, it should be highlighted that there are interactions between species. For example, in cases where seagrass beds are more sensitive than seaweed meadows, increases in nutrient levels in the water column due to human activity can lead to significant increases in seaweed meadows that can negatively affect seagrass populations [15]. Thus, in some areas where ecosystems are in delicate equilibrium, human activity can be catastrophic.

The study area of the work corresponds to the Port of Granadilla (Tenerife Island, Canary Islands, Spain) and nearby areas in open Atlantic oceanic waters (Figure 1a). The port area has a total marine surface of approximately 1.2 km². Specifically, the aim is to study the anthropogenic impact and potential threats of the construction of a large industrial port on the seabed near the highly biodiverse Special Area of Conservation (SAC) Natura 2000 of the *Cymodocea nodosa* beds in the South of Tenerife Island. In addition to the *Cymodocea nodosa*, the area also has other seabed species, such as a large expanse of *maërl* or *Caulerpa prolifera*, among others. On the other hand, Figure 1b shows the zone, where the yellow dashed box displays the selected study area. The green areas show the historical population of *Cymodocea nodosa* [16]; the orange parallel lines show the new Port of Granadilla; and, finally, the blue transverse lines show the Natura 2000 SAC. It can be observed that the port is outside the SAC, but, as highlighted in the results, the SAC is also affected by the construction of the port. In addition, note that the historical *Cymodocea nodosa* meadows extend outside the SAC, even in a higher population than inside the SAC, so *Cymodocea nodosa* is equally or more important in the port area.

Remote sensing is positioned as a useful tool for biodiversity monitoring due to its ability to obtain temporal data over large areas in a cost-effective and temporally accessible way compared to other types of data capture approaches, such as in situ measurements [17,18]. In particular, the use of very-high-resolution (VHR) satellite images provides sufficient resolution to significantly monitor changes in the seabed [19]. In addition, multispectral satellite sensors allow for classifying and distinguishing different types of seabeds by their spectral behavior [20]. Additionally, the use of supervised machine learning classification methods allows for very-high-quality maps to be obtained [21].

In this work, three WorldView-2 (WV-2) satellite images (before, during, and after the construction of the Port of Granadilla) were selected to assess the impact of the port's construction on seagrass and seaweed meadows in the short term due to human impact. As the first stage of the developed methodology, advanced pre-processing models were applied to mitigate the effects of the atmosphere, solar reflection, and image banding. In turn, maps of benthic habitats or seabed types were obtained using supervised machine learning classification techniques with the K-Nearest Neighbors (KNN) model [22]. Bathymetric maps with the Sigmoid model were also estimated and presented [23].

To the authors' knowledge, this paper is the first work that temporally observes the effects of the construction of a large industrial port in a challenging protected area of

high biodiversity through VHR satellite imagery using machine learning classification of the seabed.

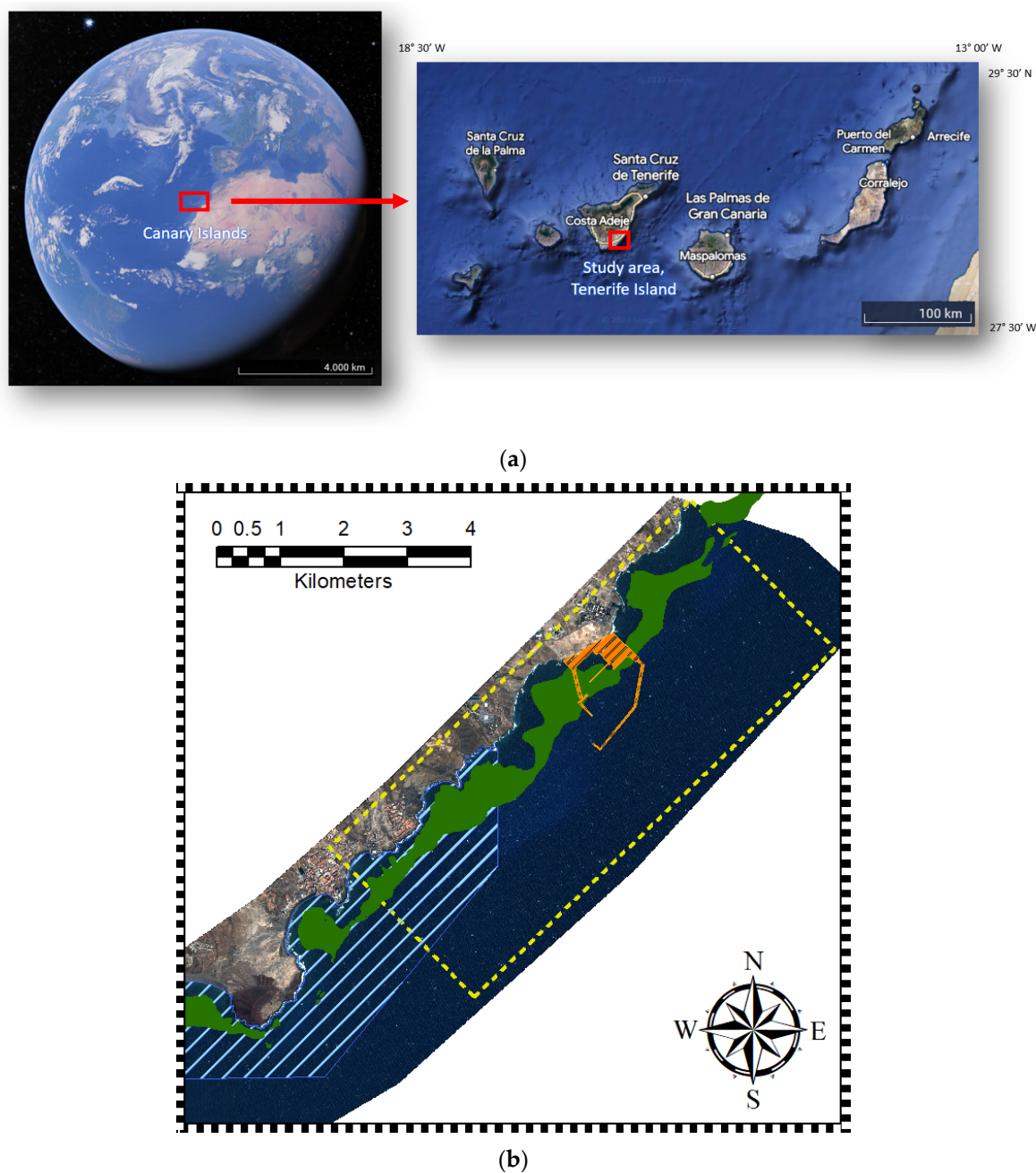


Figure 1. Granadilla Port: (a) Granadilla coast in Tenerife Island, Canary Islands (Google Earth ©), and (b) study area.

2. Materials and Methods

2.1. Study Area

In this context, the study area corresponds to the Industrial Port of Granadilla on the Island of Tenerife (Canary Islands, Spain). The port is located near the Special Area of Conservation *Cymodocea nodosa* meadows in the South of Tenerife Island (“Sebadales del Sur de Tenerife”, SAC—ES7020116). Sebadales corresponds to the canary name for the seagrass meadows of *Cymodocea nodosa*. Seagrasses are divided into six geographic bioregions [10]: Temperate North Atlantic, Tropical Atlantic, Mediterranean, Temperate North Pacific, Tropical Indo-Pacific, and Temperate Southern Oceans. Specifically, the

species considered in this work correspond to the Mediterranean bioregion. Regarding the species of *Cymodocea nodosa*, it is the species present in the Canary Islands, *Cymodocea nodosa* (*Ucria*) *Ascherson*. In addition, in this area, there is a wide variety of species, such as *maërl* beds of *Lithothamnion corallioides*, and the algae *Caulerpa prolifera* is also present. Specifically, regarding *maërl*, it is important to note that they are non-renewable structures due to their slow growth of 1 mm per year [24–26]. They are highly sensitive, and if the present meadow conditions are lost, they may not be recoverable over an extended period. In addition, the area includes other species, such as photophilous algae and various seabed habitats, such as sand or deserted areas of rock without vegetation called *blanquizal*.

It is remarkable that the Port of Granadilla is the largest exclusively industrial port in the Canary Islands, with a marine surface area of 1.2 km². Therefore, as mentioned above, the construction of a port of this size could have a negative impact on biodiversity. Consequently, it is necessary to monitor its impact over time to be able to assess the possible interactions with the environment and its biological stability. For this reason, the founding purpose of the Observatorio Ambiental Granadilla (OAG) foundation is to ensure that the port is managed in an environmentally friendly manner, monitoring the status and trends of local biodiversity while ensuring the appropriate application of corrective and compensative measures.

2.2. Data

Three very-high-resolution multispectral WorldView-2 satellite images were taken of the study area. The WV-2 images had an 8-band multispectral sensor covering the blue to infrared spectral range (400–1040 nm) with a radiometric resolution of 11-bit values. Furthermore, the spatial resolutions depend on the image off-nadir platform sensing angle: 2.0 m for 2011, 1.8 m for 2014, and 1.9 m for 2022. These differences are considered in the final comparison of the results.

The imagery selected corresponds to a date before the port's construction on 18 September 2011 (Figure 2a), another during the port's construction on 22 September 2014, at the start of the works of the main breakwater and the counter-dike (Figure 2b), and, finally, another at the end of the main works of the port's construction on 23 October 2022 (Figure 2c).

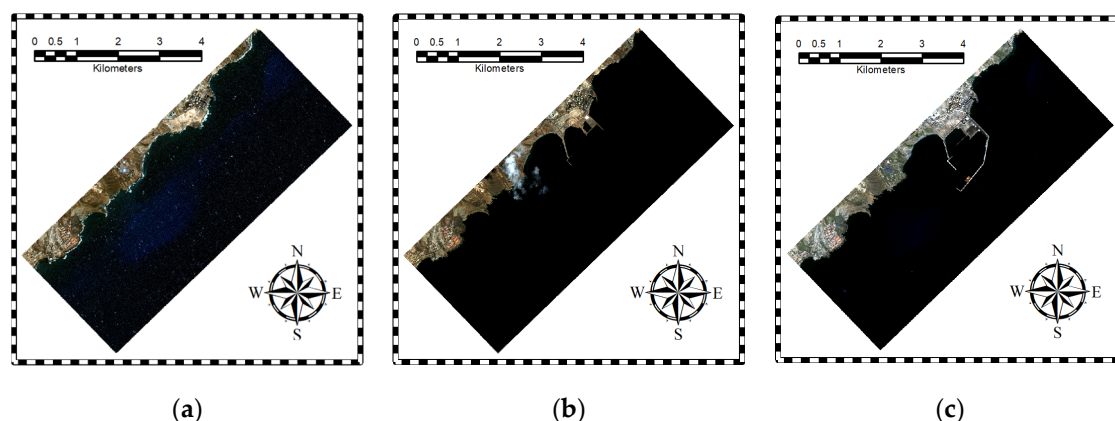


Figure 2. Satellite imagery of the study area: (a) 18 September 2011, (b) 22 September 2014, and (c) 23 October 2022.

A pre-selection among a total of 23 images from July 2011 to October 2022 was performed by pre-processing and qualitatively analyzing them all. It is noteworthy that the study area is an open sea area with quite a rough water surface and a significant presence of inorganic matter due to port construction and activities, which corresponds to a Case-2 water type [27]. Only summer images were considered, discarding winter images. This selection avoids errors in the interpretation of the results since it avoids the seasonality

of the marine species. For example, *Cymodocea nodosa* has a higher growth and density during summer. Thus, mixing images from different seasons would generate errors in the population estimates since the effect of growth or decline would not only be affected by the port. This choice makes it possible to ensure that changes are mainly due to the construction of the port. The summer season is chosen to maximize the growth of the species, allowing better observation of the impact of the port using satellite data. Finally, the three best images were selected to observe the impact before, during, and after the port's construction.

Supervised machine learning classification models were used to generate the benthic maps. The selection of the bottom classes or types in the classification, as well as the selection of the Regions of Interest (ROIs) of the datasets, were carried out with specialist biologists and transects captured by the staff of the OAG. A total of 12 bottom types have been discriminated: *Cymodocea nodosa* (sparse, medium, and dense), *maërl* (pure and mixed), *Caulerpa prolifera*, photophilic algae, sand, *blanquizal*, calcareous, muddy water, and deep water. Specifically, *blanquizal* is understood as shallow rocky substrates that are dominated by the presence of the sea urchin *Diadema antillarum*, and calcareous is understood as a seabed which is composed of calcium carbonate and is usually stony and yellowish white in color. The maps obtained classify the seabed up to a depth of 25 m. Some examples of the most relevant classes of *Cymodocea nodosa*, *maërl*, and *Caulerpa prolifera* in the study area are shown in Figure 3.

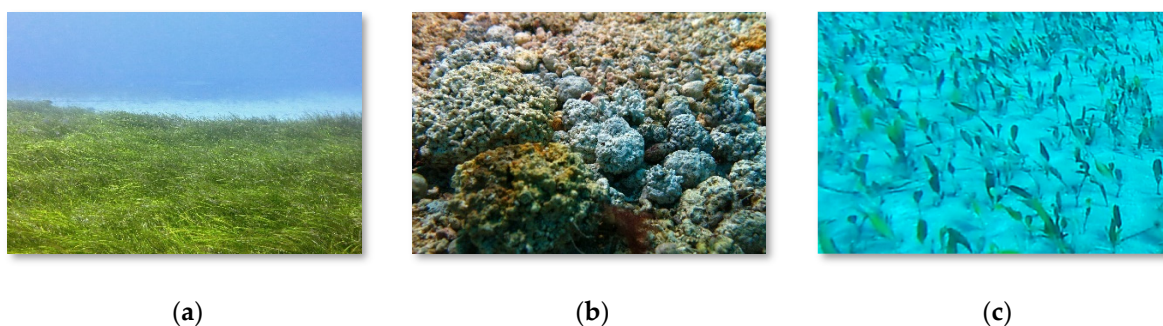


Figure 3. Examples of (a) dense *Cymodocea nodosa*, (b) pure *maërl*, and (c) *Caulerpa prolifera* in the study area.

Based on the collected ROIs, all pixels are extracted to obtain the total dataset. Then, the data are divided into two groups: training and test datasets. Both datasets are obtained from the initial set, which is divided into 80% for training and 20% for testing. Uniform random sampling was used for the split. Regarding the total samples, it can be commented that for the 2011, 2014, and 2022 images, there are a total of 195.637, 302.892, and 189.474 sample pixels, respectively. It should be highlighted that the division into train and test datasets is made in each class to maintain the distribution of the data. In addition, several zones were chosen across all depths in the selection of ROIs. This allows the training models to consider the effects of the water column [22]. Figure 4 shows the distribution of the samples in relation to depth for each image and seabed type. The commented distribution refers to the training and test data, but it is a good indicator of the final distribution of the different species in the final maps.

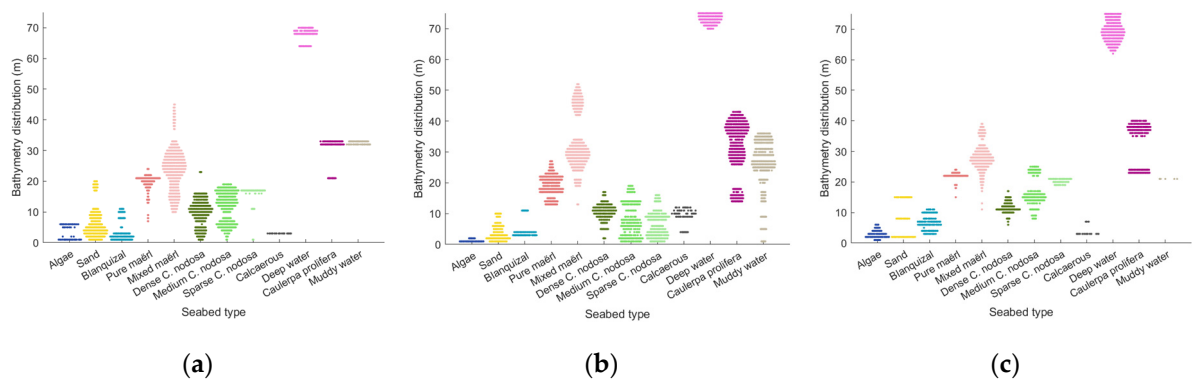


Figure 4. Distribution of sample pixels in relation to depth for each seabed type and image: (a) 18 September 2011, (b) 22 September 2014, and (c) 23 October 2022.

2.3. Imagery Processing

Due to the nature of passive remote sensing, where only sunlight re-emitted by the surface is received, the images obtained are subject to a variety of unwanted effects or noise. Therefore, pre-processing techniques are applied to remove the noise that degrades the quality of the results. Then, seabed type maps are generated using supervised machine learning techniques. Finally, a comparison of the resulting images is performed to evaluate the temporal evolution of the seabed types. The general methodology of the work is presented in Figure 5.

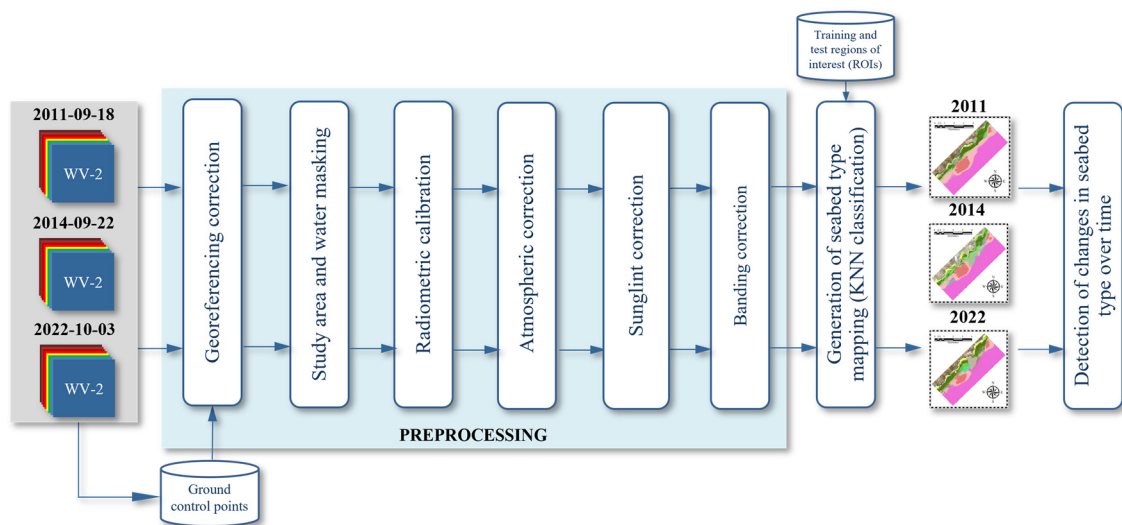


Figure 5. Methodology for the generation of seabed type mapping.

2.3.1. Pre-Processing

- Georeferencing correction

Initially, georeferencing correction must be carried out. In the original WorldView-2 images, it has been detected that, in some cases, there is a spatial deviation with respect to the reference. For the correction, reference ground points are used, and a first-order polynomial transformation is applied. It bears mentioning that this pre-processing step is essential in the comparison of the maps, as well as in the generation of the maps.

- Study area and water masking

It should be highlighted that the three original images differed in terms of their geographical extent. Initially, the pixels corresponding to water areas were extracted using the Normalized Difference Water Index (NDWI) [28], and the mask was generated

empirically by a thresholding. Later, all the images were masked to a common area, which includes the study region shown in Figure 1.

- Radiometric correction

Subsequently, to convert the image to physical values, the digital numbers acquired by the analogue to digital converter of the satellite sensor were converted to values of radiance at the top of the atmosphere (ToA). For this, the linear model was used with the values provided in the metadata file (.IMD) attached to the WorldView-2 images and provided by DigitalGlobe (Westminster, CO, USA) [29].

- Atmospheric correction

The subsequent processing step corrects atmospheric effects, such as absorption and scattering. From the ToA radiance values, the reflectance values at the bottom of the atmosphere are obtained. The atmospheric correction is a complex pre-processing, due to the non-uniformity of the atmosphere, as well as the fact that it is a non-linear and time-varying system [30]. An extensive study on the use of various atmospheric correction models was previously carried out [31,32], where it was shown that the 6S (Second Simulation of a Satellite Signal in the Solar Spectrum) model [33] achieves the best results for the case study. A maritime aerosol profile, a mid-latitude summer atmospheric profile, a clear water reflectance profile, a surface altitude of 0 m, as this is a marine application, and image-dependent Atmospheric Optical Thickness (AOT) information were used for the correction. An AOT value of 0.08 was used for the 2022 image, 0.04 for the 2014 one, and 0.13 for the 2022 one.

- Sun glint correction

Later, the effect of sun glint on the sea surface, which produces brightness in the image due to the specular reflectance of sunlight caused by waves on the sea surface [34], must be considered. There is a multitude of methods to mitigate the effect of sun glint, where information from the infrared bands is used, as there is a large scattering of visible light at these wavelengths, allowing the brightness components to be obtained clearly. Two of the most widely used models are those proposed by Lyzenga et al. [35] and Hedley et al. [36]. Both models are based on the suppression of the brightness component by the relation between visible and near-infrared (NIR) bands. In Lyzenga, the relation is performed statistically, while in Hedley, it is performed through a linear regression. In this work, the correction is obtained using Hedley's algorithm. Figure 6 shows the correction in the image of 18 September 2011, which corresponds to the highest sun glint case. In addition, it is worth mentioning that the optical instrument of the WorldView-2 satellite is divided into two multispectral sensors: MS1 and MS2. The MS1 group consists of the blue (2), green (3), red (5), and near-infrared 1 or NIR1 (7) channels, while the MS2 group consists of the coastal blue (1), yellow (4), edge red (6), and NIR2 (8) channels. There is a time difference of approximately 0.26 s between both sensors [37]. For this reason, there may be spatial offset in objects that are in appreciable motion, and relative to the capture time delay, as in the case of solar glint due to waves. Therefore, the corresponding infrared channel of its multispectral sensor is used for the correction of the associated visible channels. In other words, NIR1 is used for the blue, green, and red channels and NIR2 is used for the blue coast, yellow, and red edge channels.

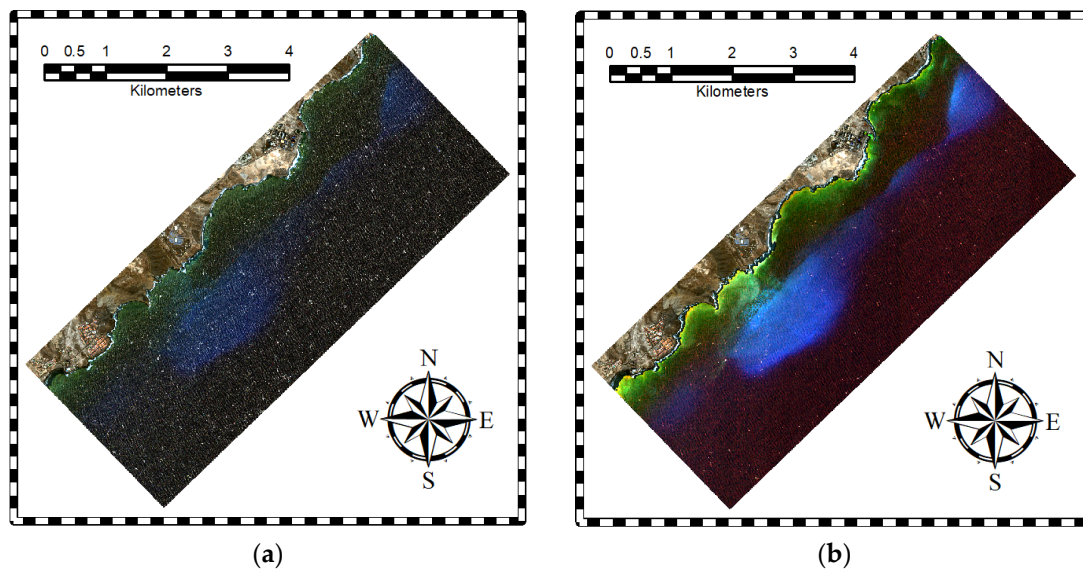


Figure 6. Results of the sunglint correction on the image of 18 September 2011: (a) image without the application of the sunglint correction and (b) image with the Hedley correction.

- Banding correction

Finally, a correction of the banding produced by the radiometric difference between satellite sensors was performed [38]. In this case, the vertical banding property was used to correct the banding. Intensity jumps were used to equalize the image. Figure 7 shows the application of the banding correction for the study image of 3 October 2022.

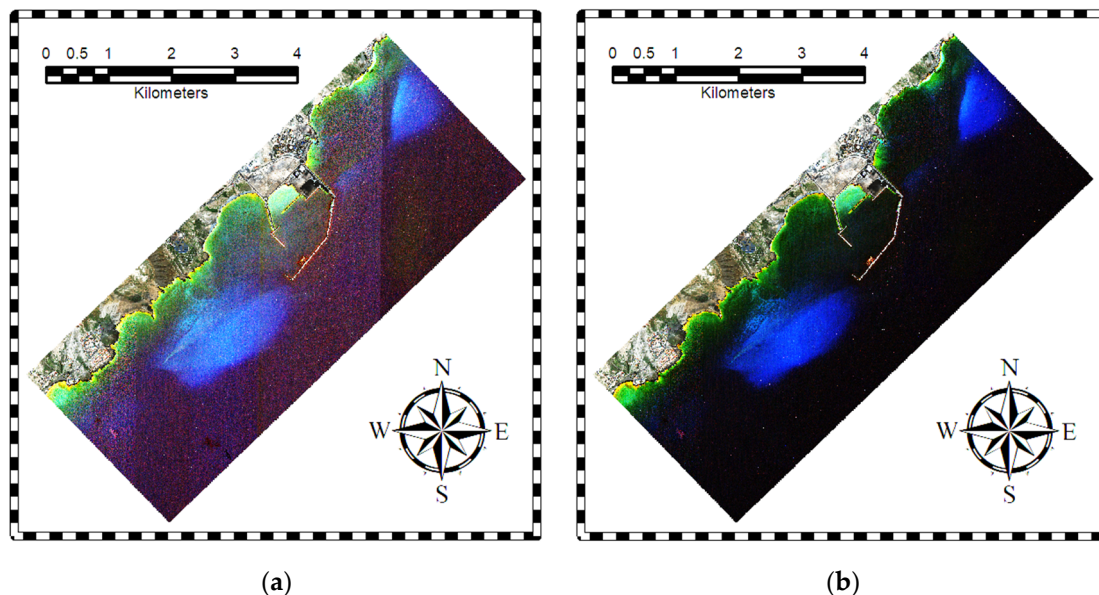


Figure 7. Results of the banding correction on the image of 3 October 2022: (a) image without the banding correction and (b) image with the banding correction. In both images, the brightness has been increased by 20% and the contrast by 40% to highlight the impact of the pre-processing.

The results of the pre-processed images are presented in Figure 8. Compared to the original images in Figure 2, a higher detectability of the seabed is observed. For example, the light blue areas are due to the high reflectivity of the *maërl*. In the annotated figure included in the results, a reduction in mostly *maërl* composite meadows is visible.

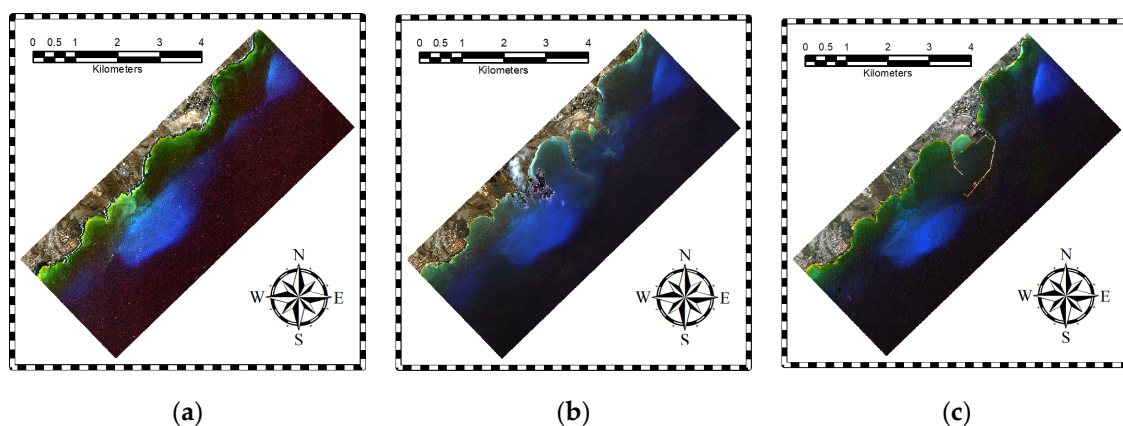


Figure 8. Pre-processed images for (a) 18 September 2011, (b) 22 September 2014, and (c) 3 October 2022.

2.3.2. Classification

In benthic mapping using remote sensing satellite imagery, the traditional maximum likelihood algorithm normally provides good results [39]. However, in the last decade, supervised machine learning techniques have been mostly considered. Popular methods in this category are decision trees, random forest, Support Vector Machine (SVM), and K-Nearest Neighbors (KNN) [39,40]. After a preliminary review of the classification techniques, the results were quite similar, with KNN [41] giving excellent results. For this reason, KNN was chosen to generate the mentioned seabed maps.

In a previous study [26], and in the same study area, the impact of water column correction methods and various classification algorithms was analyzed. It was found that, for complex waters down to considerable depths, the performance of the correction models was not satisfactory. Therefore, if there are training data available at different depths, not using water column correction methods obtains better results. In addition, it was also found that using the eight WorldView-2 channels improves the results. On the other hand, among the classification algorithms used, KNN was positioned as one of the best algorithms, along with Support Vector Machine with Gaussian kernel [23,42].

Compared to deep learning methods [43], traditional or machine learning techniques obtain maps of higher accuracy because a large training dataset is not available [43]. In addition, these methods can be more independent on data errors by avoiding over-fitting on small datasets. In any case, future work in deep learning should be carried out, focusing on transfer learning techniques [44].

Finally, the 2022 result masked out the inner port with the muddy water class. Since this area was assured by the OAG foundation experts to be a muddy bottom after the port's construction, the ROIs inside the harbor were removed to decrease the variance of the muddy waters class and improve the classification results. After classification, a 5×5 pixel median filter was applied to reduce impulsive noise in the results.

To evaluate the results, a qualitative and a quantitative analysis was carried out. For the qualitative analysis, the maps obtained are included. Moreover, for the quantitative analysis, the confusion matrices are presented, as well as the recall, precision, and F_1 score metrics.

2.3.3. Detection of Changes in Seabed Type over Time

Lastly, the results obtained on the three dates are compared in relation to the construction of the port. As mentioned above, the spatial resolutions are 2.0 m, 1.8 m, and 1.9 m for the 2011, 2014, and 2022 images, respectively. Therefore, to compare the three images, the resolution of the images is reduced to the lowest resolution of 2.0 m. The Nearest Neighbor interpolation method [45] is used since the results of the maps are discrete. As

a last step, the number of pixels of each seabed class is counted, and the surface area is obtained considering the spatial resolution.

3. Results

This section presents the main results of the work divided into two groups. Firstly, the results of the seabed type maps are shown, where the maps, along with the metrics and confusion matrices, are presented. Secondly, the temporal comparison, representing the evolution of the surface area, is also shown.

3.1. Seabed Maps

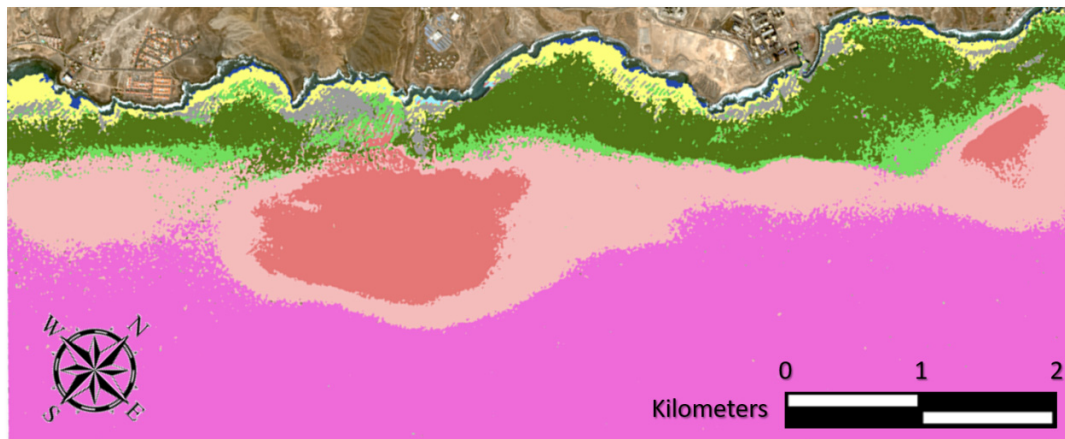
Figure 9 shows the maps resulting from the classification of bottom types for the study area. The large number of classes that have been classified in this challenging Case-2 and deep complex waters is highlighted. A notable decrease in the *maërl* surface can be seen, both mixed and pure. In addition, the appearance of muddy waters from the port works can be seen, as well as the appearance of new meadows of the species *Caulerpa prolifera*, where its population congregates notably at the entrance to the Port of Granadilla. Specifically, regarding muddy waters, note that in 2014, there was great turbulence due to the construction of the port along the entire area. However, in 2022, muddy waters were concentrated inside the port. Finally, regarding the *Cymodocea nodosa*, disappearance of the meadows that existed before construction in the port area can be seen.

In terms of quantitative results, the error metrics are first presented and summarized in Table 1. High performance values can be seen for all metrics. The 2014 map has the best recall metric with 77% compared to the 2011 and 2022 maps with 76%. Parallely, the 2011 map has the best precision with 85% compared to 2014 with 81% and 2011 with 80%. Finally, for the F₁ score metric, 2011 yields the best score with 80%, followed by 2014 with 79% and 2022 with 77%. All metric values are high and, therefore, the benthic maps derived from the WV-2 imagery are of high quality. The biologists of the OAG have also validated the results.

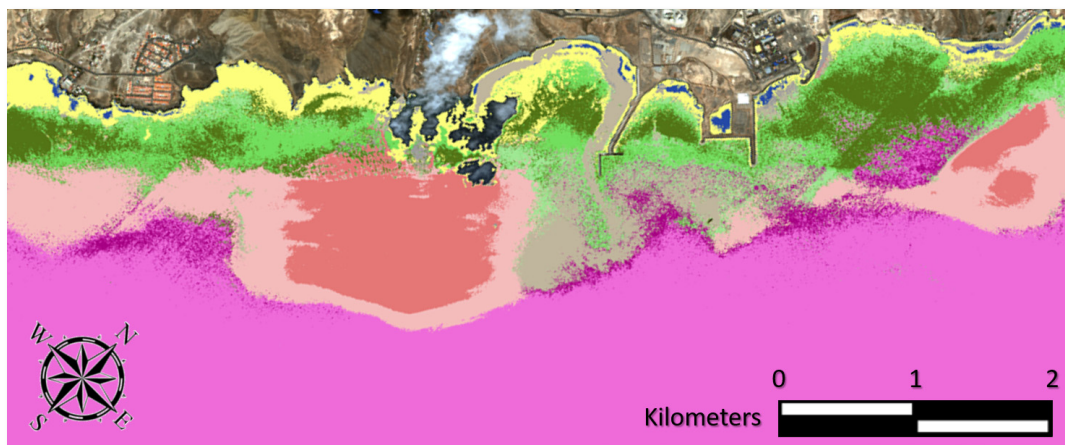
Table 1. Quality metrics of the seabed type maps. Bold indicates the best value for each metric in the different years, and the up arrow indicates that the metric value should be as large as possible.

Date	Recall ↑	Precision ↑	F ₁ Score ↑
18 September 2011	76%	85%	80%
22 September 2014	77%	81%	79%
3 October 2022	76%	80%	77%

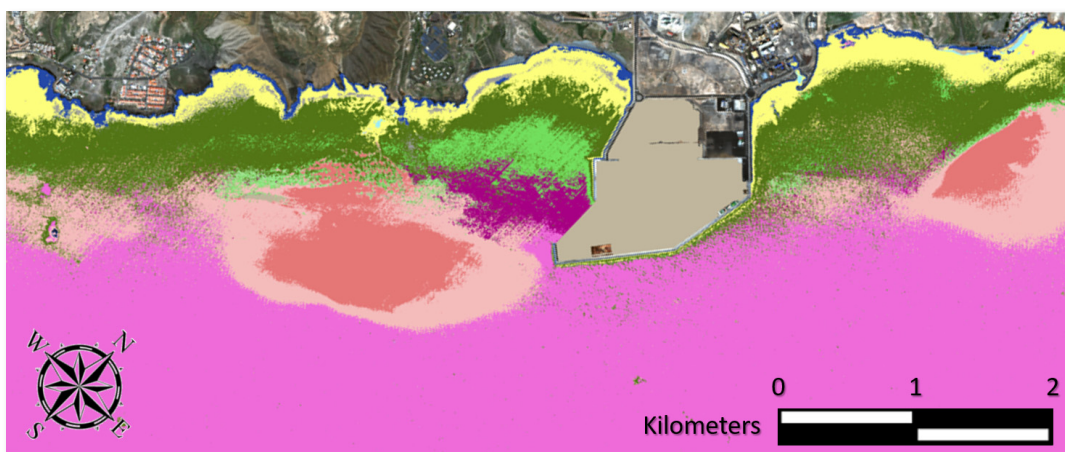
The confusion matrices expressed as percentages for the maps of 18 September 2011 (Table 2), 22 September 2014 (Table 3), and 3 October 2022 (Table 4) are presented, where the numbering used corresponds to that in Figure 9. In general, it can be noticed that high separability has been achieved among most of the classes. *Maërl*, *Cymodocea nodosa*, sand, and calcareous classes can be highlighted. In addition, the confusion between *maërl* types and *Cymodocea nodosa* types should also be emphasized. In this aspect, it should be noted that the maps obtained have been validated with OAG experts, and confusion is due to some ROIs positioned in areas of great challenge for the algorithm, the great spectral similarity, and the limits of satellite multispectral imagery acquisition technology. Additionally, confusion between the *Caulerpa prolifera* and mixed *maërl* classes can be observed since the mixed *maërl* definition includes this species, among others. The values obtained are expected and validate the maps.



(a)



(b)



(c)



Figure 9. Results of the seabed type maps obtained with the KNN model for (a) 18 September 2011, (b) 22 September 2014, and (c) 3 October 2022.

Table 2. Confusion matrix as percentages for the map of 18 September 2011.

		Predicted Class											
		1	2	3	4	5	6	7	8	9	10	11	12
True Class	1	78.5	17.1				1.9		2.5				
	2	18.5	67.6				8.8						5.1
	3	3.5	3.8	65.2			24.0						3.5
	4				79.9				20.1				
	5					97.6	2.4						
	6					5.5	88.5						6.0
	7							93.1	6.9				
	8	4.5	4.6						90.9				
	9		9.3						10.6	80.1			
	10		6.8				17.6				37.8		37.8
	11			28.5			24.7					46.8	
	12		2.6				6.8						90.6

Table 3. Confusion matrix as percentages for the map of 22 September 2014.

		Predicted Class											
		1	2	3	4	5	6	7	8	9	10	11	12
True Class	1	75.6	12.8	6.7					4.9				
	2	14.7	62.1	10.7					5.8		6.7		
	3	16.3	16.7	53.7					7.1		6.2		
	4				72.2			2.2	16.1		9.5		
	5					96.6	2.7				0.7		
	6					5.9	87.3				4.2	2.6	
	7			1.5				84.1	14.4				
	8	3.6	2.6	4.0				4.4	85.4				
	9					28.4				71.6			
	10			2.9			5.9				86.9	4.3	
	11		3.8	3.0			11.8				9.1	55.0	17.3
	12						0.7					2.5	96.8

3.2. Temporal Evolution of the Seafloor

At last, the temporal evolution of seabed types in Granadilla is presented and discussed. Figure 10 shows the seabed evolution of the study area. In Figure 10a, the results are shown comparing a crop of 2011 and 2022 as an example, with the same color palette as in Figure 9. It is important to highlight that the analysis was performed on the whole image, not only on the crop shown in Figure 10a. On the other hand, Figure 10b illustrates the evolution of the surface area of each class over time. In this case, only the most important classes are presented (total *Cymodocea nodosa*, pure *maërl*, mixed *maërl*, *Caulerpa prolifera*, and muddy waters). The remaining classes are not relevant to study biodiversity, such as deep water and sand, or their evolution has not significantly varied over time, such as the other classes of algae, *blanquizal*, and calcareous.

Table 4. Confusion matrix as percentages for the map of 3 October 2022.

	Predicted Class												
	1	2	3	4	5	6	7	8	9	10	11	12	
True Class	1	78.1	8.7		4.4				3.3			5.5	
	2	33.4	50.8				7.3		4.5			4.0	
	3	16.3	11.9	38.3			24.4					9.1	
	4	23.2	5.8		56.6				14.4				
	5					92.1	7.9						
	6					7.0	78.5					7.8	6.7
	7	2.5			2.3			95.2					
	8	3.5	1.2						95.3				
	9								13.4	86.6			
	10					6.5	6.6				86.9		
	11		2.6	2.5			27.5					52.3	15.1
	12						2.6					1.0	96.4

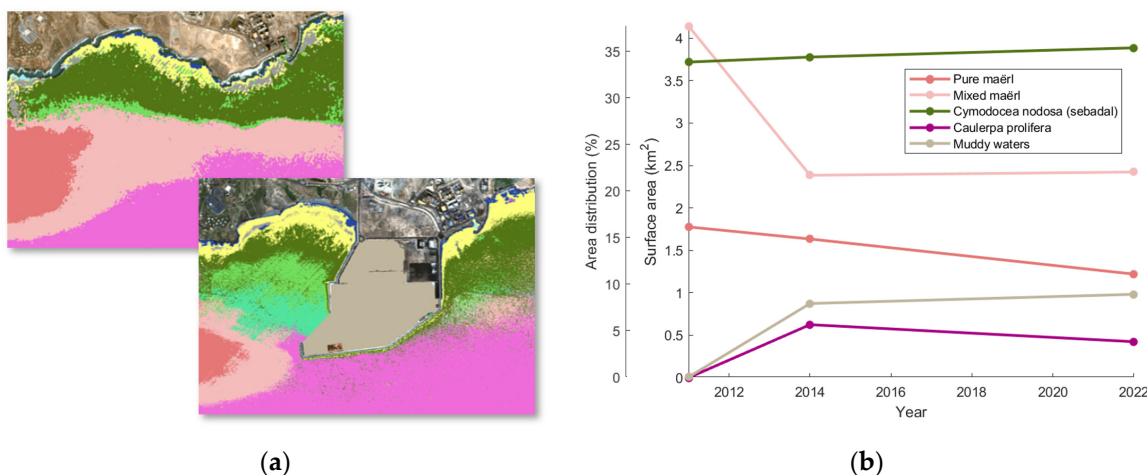


Figure 10. Evolution of the seabed types: (a) maps of 2011 and 2022 for the port area and (b) graph of surface changes for the entire area.

Regarding the results, the previous comments on *maërl* can be seen, as there has been a notable decrease in the meadows where the mixed *maërl* has been mostly affected, with a decrease of approximately 1.6 km². Concurrently, the pure *maërl* community has suffered a decrease of approximately 0.3 km². However, according to the curve described, there is a constant decrease in pure *maërl* but a stabilization of mixed *maërl*. It should be highlighted that the *maërl* has transitioned to 0.59 km² of muddy waters, due to the port, 0.87 km² of *Cymodocea nodosa*, and 0.38 km² of *Caulerpa prolifera*. Since *maërl* can be a substrate for other species, *maërl* could coexist with *Cymodocea nodosa* and *Caulerpa prolifera* without disappearing. However, due to the limitations of passive remote sensing, this phenomenon cannot be determined in this work and needs to be studied in the future with in situ measurements. On the other hand, the amount converted into muddy waters by the port is very likely not to be recoverable.

Furthermore, regarding the *Caulerpa prolifera* class, this species, which was previously scattered in the area, has become established in an extensive meadow of 0.42 km² at the entrance to the port. The relationship between the construction of the port and the year of appearance is observed, so it is very likely that its establishment as a meadow is due to

the port's construction. Notwithstanding this, there is stabilization by the year 2022. The same applies to muddy waters, which appeared in a large surface of 0.98 km² with the construction of the port and steadied inside the port in 2022.

Concerning *Cymodocea nodosa*, it is worth noting that by merging all three classes related to this phanerogam, it remains basically constant. This can be summarized by the observation that large areas of *maërl*, approximately 0.87 km², are converting to *Cymodocea nodosa*. This is an encouraging result for the conservation of this vegetal formation within the Special Area of Conservation. In addition, part of the *maërl* meadows, 0.38 km², has also been converted into *Caulerpa prolifera* meadows. It must be noted that the *maërl* is also a fundamental species in the conservation of marine fauna, as well as in the regulation of carbon dioxide in the sea, since it needs calcium carbonate in its growth, allowing for the greater absorption of carbon in the water, helping to mitigate the effects of climate change [46].

Additionally, it should be highlighted that the *Cymodocea nodosa* increase due to the deterioration of the *maërl* is counterbalanced by the loss of *Cymodocea nodosa* mostly to muddy water due to the construction of the port with 0.30 km², and to sand, which increases to 0.47 km². From the study, it is appreciated that the *Cymodocea nodosa* can only colonize *maërl*, so that, if in the future the *maërl* disappears, the *Cymodocea nodosa* may not be able to increase its population, also disappearing. Therefore, the *maërl* is not only important as a marine species for its properties but it also protects the population of *Cymodocea nodosa*.

On the other hand, regarding the direct impact of the port, it can be observed that 0.59 km² of pure and mixed *maërl* and 0.30 km² of *Cymodocea nodosa* are not detected in the 2022 image in the port area due to muddy water. It is very likely that this large expanse of meadows has disappeared due to sedimentation in the construction of the harbor.

4. Discussion

Remote sensing allows for studies of a large geographical area to be performed using an accessible and quick method compared to other approaches of data capture, such as in situ measurements. Specifically, the use of very-high-resolution multispectral passive optical satellite imagery in this case has made it possible to carry out a multitemporal analysis to study the anthropogenic impact of the construction of a large industrial port on the seabeds in a protected area.

In addition to the comments made in the previous section, regarding the results on the *Caulerpa prolifera* meadows, in [47], it was stated that sedimentation caused by turbidity, as in the case study due to the construction of the port and the presence of the outfall, can cause seaweed meadows to colonize *Cymodocea nodosa*. However, the same author [48] presented a study in which it was found that *Caulerpa taxifolia* will coexist in the long term with *Cymodocea nodosa*. Regarding the case study, it has been found that there is a correlation between the presence of muddy port water and the emergence of *Caulerpa prolifera* meadows in the short term. It is also probable that *Caulerpa prolifera* will not expand further if sedimentation does not increase and may coexist with *Cymodocea nodosa* meadows. However, *Caulerpa prolifera* can continue to expand and, in this case, the need is stressed for a particular study to be able to analyze the long term impact.

On the other hand, it should be highlighted that the most affected species have been the *maërl* meadows. As explained, the *maërl* is a formation of great biological importance, and its impact on other grasslands and species must be made relevant. As this study has shown, there is a decrease in meadows mostly detected as *maërl*, which may cause interactions with *Cymodocea nodosa* and *Caulerpa prolifera* meadows as the *maërl* may be on the bottom and hidden by leaves. This study shows that the reduction in *maërl* was exploited by *Cymodocea nodosa* to proliferate in favor of the decrease probably produced by the port. Additionally, *Lithothamnion* species have a greater difficulty in terms of regeneration due to their very low growth of 1 mm per year [24–26]. Therefore, the need for a study to observe their interactions in the Granadilla area in the long term is highlighted. In addition, sedimentological studies should be carried out in future works to analyze the possible

modification of bottoms with the presence of muddy water, and the effect it may have on the interaction between species. Another possible future work could be to investigate the modification of the current regime by the port's construction, and as it affects the seabed.

As can be seen, the impact of the port on certain species of great richness can be expected. However, the impact of the port's construction is not only limited to seabed types but also to the bathymetry, which can indirectly affect the seabeds. This may be due to the blockage of the marine current by the port dikes, modifying the depth depending on the currents. Figure 11 shows the bathymetry obtained with the Sigmoid model [26], which is an improvement on the traditional Stumpf et al. [49] model where, instead of using linear regression, a sigmoid regression is considered to model the non-linearity of the logarithmic relationship of the blue and green bands. In this case, the reference in situ bathymetry measured by the Spanish Institute of Oceanography (IEO) before the construction of the port was used, corresponding to isobaths of 1 m resolution. In addition, since the marine current is a north–south direction, the northernmost part of the study area was used for training to avoid the information being modified over time with respect to the reference. The presented pre-processed images have been used to train the bathymetric model, where the three maps have obtained Mean Absolute Errors (MAEs) of 2.54 m, 1.82 m, and 2.44 m for 2011, 2014, and 2022, respectively. On the other hand, the adjusted R^2 values of the classification were 0.79, 0.91, and 0.81 for 2011, 2014, and 2022, respectively. Low MAE values and high R^2 values were obtained in all cases, implying high-quality maps.

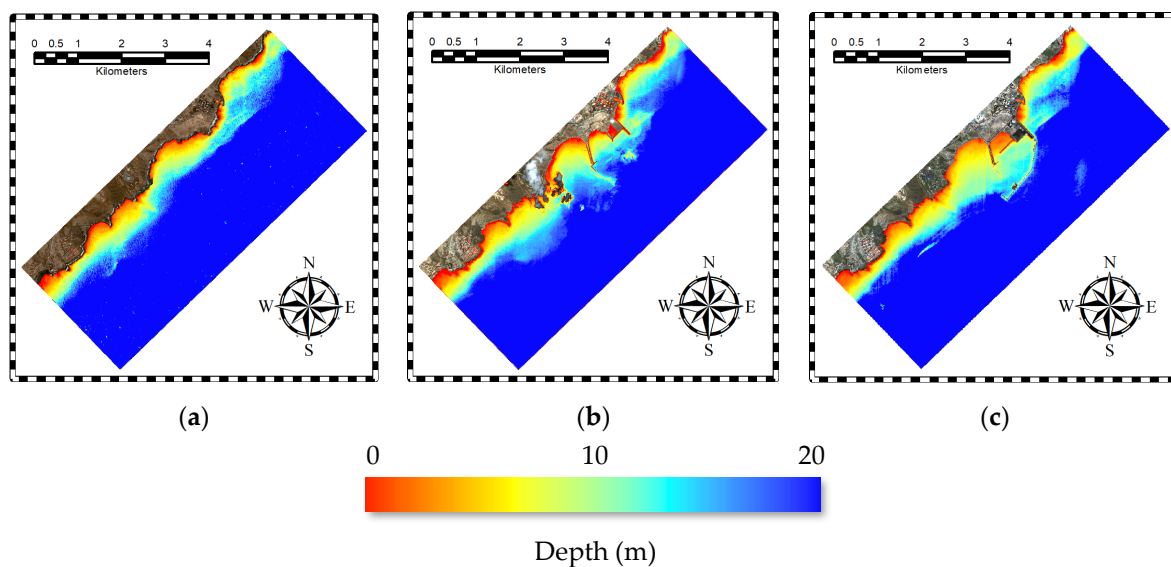


Figure 11. Bathymetric maps obtained with the Sigmoid model for (a) 18 September 2011, (b) 22 September 2014, and (c) 3 October 2022.

Regarding the results, it can initially be observed that in the inner port area, the bathymetry decreased with time due to sediment deposition from the main breakwater. On the other hand, a lower depth is also found in the southern and adjacent part of the harbor, which also indicates sediment deposition. In relation to the results of the seabed types, it can be highlighted that the material deposited in the interior of the port is sediments. On the other hand, regarding the south of the port, an observation can be made on the deposition of matter in relation to the establishment of the *Caulerpa prolifera* meadow in the area, as it can take advantage of the sediments generated in the port. It is also noteworthy that the presence of turbid water in 2014 was observed in the maps of seabed types, which may produce an anomalous bathymetry due to suspended matter.

In addition to the above, and to complete the knowledge of the anthropogenic impact in the study area, it is necessary to explain the existence of an underwater outfall of urban human wastewater. Specifically, this is the submarine outfall at the public beach of La

Batata—Ensenada de Pelada, where the source is the urban center of Arenas del Mar. It is very important to note that, as of 11 November 2021, the outfall is not authorized because the license has expired [50]. However, in Figure 12, the outfall is emitting waste on 3 October 2022. Specifically, in the area highlighted by a red box in Figure 12a, the impact of the discharge on the bathymetry can be observed, detecting abnormal shallow water in deep water areas. This is due to the suspended matter emitted, which is found to be along the water column and not only at the bottom. Figure 12b shows the pre-processed image where the outfall emission along the *maërl* meadow towards the harbor can be seen. Thus, the complexity of the study area is exposed, where the anthropogenic effect is not only limited to the construction of the harbor.

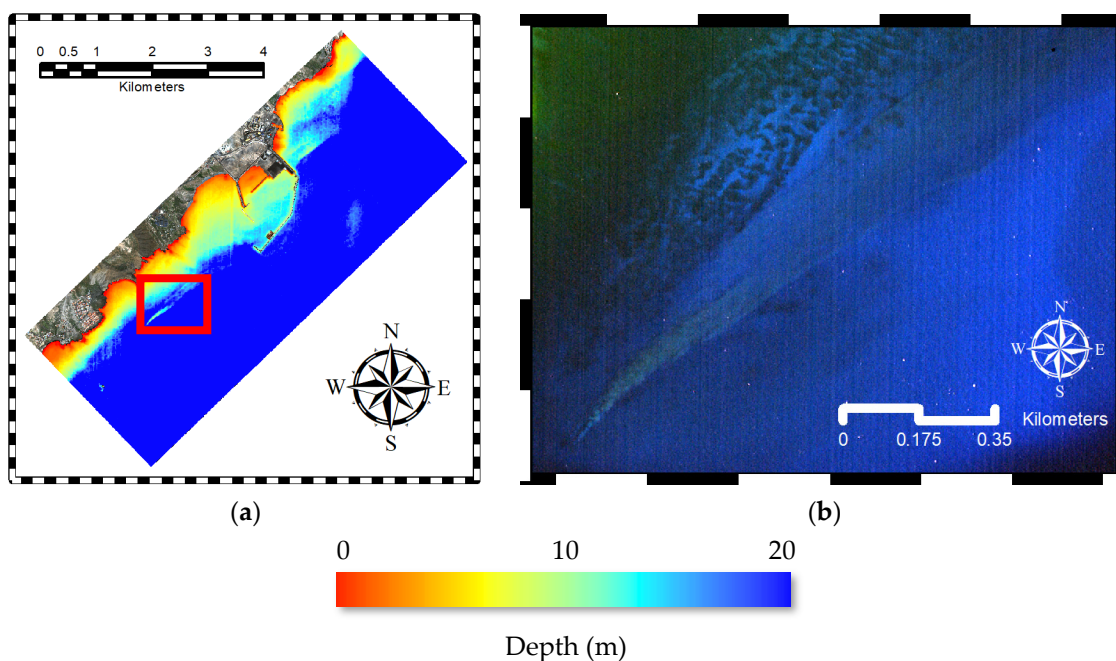


Figure 12. Unauthorized submarine outfall emitting urban human sewage in the 3 October 2022 image: (a) bathymetric map showing the abnormal shallow depth due to the outfall (the area is highlighted in a red rectangle), and (b) outfall emission in the original image.

Finally, and unfortunately, it is relevant to note that this type of activity is common in the Canary Islands. In the General Report of the Canary Islands on the census of outfalls from land to the sea in the Canary Islands in 2021 [51], dated March 2022, it is expected that the number of total outfalls is 434, with an increase of 40 compared to 2017, of which 48% of the outfalls are not authorized. However, some of these unauthorized outfalls do emit, as can be seen. Specifically, on the island of Tenerife, the total number of emitters is 195, which corresponds to approximately 45% of the emitters in the Canary Islands, and of which 37% of the emitters are not authorized. In addition, it must be said that there are still illegal and unaccounted for outfalls. Regarding the impact, it is worth remarking the work of Pérez-Fernández [52], which analyses the impact of an underwater outfall on the neighboring island of Gran Canaria. The work highlights that *Cymodocea nodosa* is affected by the outfall due to the turbidity factor and epiphytism, and probably due to changes in salinity. Furthermore, it is stated that *Caulerpa prolifera* indicates higher resistance than *Cymodocea nodosa*. Therefore, in addition to the clear effect of the turbidity produced by the port, the outfall may affect the *Cymodocea nodosa* seagrass meadows, as well as to the establishment of the *Caulerpa prolifera* meadow at the port entrance. In this context, future work should be carried out to observe the number and duration of episodes of emissions from both the submarine outfall and the port, and the effects on the seabed.

5. Conclusions

In this work, the anthropogenic impact of the construction of a large industrial port, the Port of Granadilla near the Special Area of Conservation of the Southern Sebedales (*Cymodocea nodosa*) of the island of Tenerife, Canary Islands, has been studied. Data from the WorldView-2 satellite were used, selecting three images before, during, and after the construction of the port in the years 2011, 2014, and 2022, respectively, to observe the short-term impact. After the application of precise pre-processing techniques, maps of seabed types were obtained with the K-Nearest Neighbors supervised classification method with a total of 12 classes of seabeds. Furthermore, classes were discriminated up to approximately 25 meters in depth in complex waters of Case-2 classes. In addition, bathymetric maps were obtained with the Sigmoid model to observe the impact of the port's construction on sedimentation. The presence of a submarine outfall was also highlighted, which may affect the seabed evolution due to the turbidity generated, in addition to the construction of the port.

After the analysis of the results, it could be concluded that high-quality maps were obtained in a challenging scenario that allows us to observe the impact of the port in the short term. Regarding the multitemporal analysis, it could be observed that the construction of the port produced a large amount of turbidity and sedimentation, which presumably affected seabed types, especially the *maërl* population, which was reduced in an area of approximately 1.9 km². In this aspect, the very low growth of the *maërl* stands out, which could mean the non-recovery of this species, as well as the fauna and micro-organisms that it contained in the area. In addition, the presence of an underwater outfall should be highlighted, which could have a negative effect due to the turbidity generated by punctual discharges. Regarding the *Caulerpa prolifera*, it was found that, most likely due to the construction of the port, a meadow of this species has appeared at the entrance to the port, colonizing part of the *Cymodocea nodosa* and *maërl* meadows. Finally, *Cymodocea nodosa* was found to have a stable population in the study area over the 11 years considered. It should be highlighted that a considerable amount of the meadows was lost due to the construction of the port; however, *Cymodocea nodosa* was able to colonize part of the *maërl* meadows that were disappearing. Therefore, it was possible to observe the short-term impact of the port's construction on the rich ecosystem, where the resilience of the environment can be appreciated despite human activities. Future work should be undertaken with in situ measurements to observe the long-term impact of the port or studying the effect of the number of emission and sedimentation episodes from the port and the submarine outfall on the meadows, as well as applying deep learning techniques in the classification of seabed maps.

Author Contributions: Conceptualization, A.M.-B.; data curation, A.M.-B.; formal analysis, A.M.-B.; investigation, A.M.-B.; methodology, A.M.-B., J.S. and J.M.; project administration, J.M.E. and F.E.; resources, J.S., J.M., J.M.E. and F.E.; software, A.M.-B.; supervision, J.M.E. and F.E.; validation, A.M.-B., J.S. and J.M.; visualization, A.M.-B.; writing—original draft, A.M.-B.; writing—review and editing, A.M.-B., J.S., J.M., J.M.E. and F.E. All authors have read and agreed to the published version of the manuscript.

Funding: This research received no external funding.

Data Availability Statement: WorldView-2 imagery is not available for open public dissemination but may be ordered through Maxar (DigitalGlobe).

Acknowledgments: This work has been carried out thanks to the support of the Observatorio Ambiental Granadilla (OAG), Contract 1-SERV-CM-2021, and for the European MAC-CLIMA project (MAC2/3.5b/254).

Conflicts of Interest: The authors declare no conflicts of interest.

References

1. Green, E.P.; Short, F.T. *World Atlas of Seagrasses*; University of California Press: Berkeley, CA, USA, 2003.

2. Hemminga, M.A.; Duarte, C.M. *Seagrass Ecology*; Cambridge University Press: Cambridge, UK, 2000.
3. Björk, M.; Short, F.; Mcleod, E.; Beer, S. *Managing Seagrasses for Resilience to Climate Change (No. 3)*; IUCN: Gland, Switzerland, 2008.
4. Duarte, C.M.; Cebrián, J. The fate of marine autotrophic production. *Limnol. Oceanogr.* **1996**, *41*, 1758–1766. [[CrossRef](#)]
5. Duarte, C.M. The future of seagrass meadows. *Environ. Conserv.* **2002**, *29*, 192–206. [[CrossRef](#)]
6. Orth, R.J.; Curruthers, T.J.B.; Dennison, W.C.; Duarte, C.M.; Fourqurean, J.W.; Heck, K.L.; Hughes, A.R.; Kendrick, G.A.; Kenworthy, W.J.; Olyarnik, S.; et al. A global crisis for seagrass ecosystems. *BioScience* **2006**, *56*, 987–996. [[CrossRef](#)]
7. Dunic, J.C.; Brown, C.J.; Connolly, R.M.; Turschwell, M.P.; Côté, I.M. Long-term declines and recovery of meadow area across the world's seagrass bioregions. *Glob. Chang. Biol.* **2001**, *27*, 4096–4109. [[CrossRef](#)]
8. Espino, F.; Tuya, F.; Blanch, I.; Haroun, R.J. *Los Sebadales en Canarias. Oasis de Vida en los Fondos Arenosos*; BIOGES, Universidad de Las Palmas de Gran Canaria: Las Palmas de Gran Canaria, Spain, 2008; 45p.
9. Trenberth, K. Uncertainty in hurricanes and global warming. *Science* **2005**, *308*, 1753–1754. [[CrossRef](#)]
10. Short, F.T.; Dennison, W.C.; Carruthers, T.J.B.; Waycott, M. Global seagrass distribution and diversity: A bioregional model. *J. Exp. Mar. Biol. Ecol.* **2007**, *350*, 3–20. [[CrossRef](#)]
11. Overpeck, J.T.; Otto-Bliesner, B.L.; Miller, G.H.; Muhs, D.R.; Alley, R.B.; Kiehl, J.T. Paleoclimatic evidence for future ice-sheet instability and rapid sea-level rise. *Science* **2006**, *311*, 1747–1750. [[CrossRef](#)]
12. Sunny, A.R. A review on effect of global climate change on seaweed and seagrass communities. *Int. J. Fish. Aquat. Sci.* **2017**, *28*, 8.
13. Wiencke, C.; Bischof, K. Seaweed biology. *Ecol. Stud.* **2012**, *219*. [[CrossRef](#)]
14. Harley, C.D.; Anderson, K.M.; Demes, K.W.; Jorve, J.P.; Kordas, R.L.; Coyle, T.A.; Graham, M.H. Effects of climate change on global seaweed communities. *J. Phycol.* **2012**, *48*, 1064–1078. [[CrossRef](#)]
15. Short, F.T.; Burdick, D.M.; Kaldy, J.E. Mesocosm experiments quantify the effects of eutrophication on eelgrass, *Zostera marina* L. *Limnol. Oceanogr.* **1995**, *40*, 740–749. [[CrossRef](#)]
16. Ruiz, J.M.; Guillén, J.E.; Ramos-Segura, A.; Otero, M.M. *Atlas de las Praderas Marinas de España*; Instituto Español de Oceanografía: Madrid, Spain, 2015.
17. Horning, N.; Robinson, J.A.; Sterling, E.J.; Turner, W. *Remote Sensing for Ecology and Conservation: A Handbook of Techniques*; Oxford University Press: Oxford, UK, 2010.
18. Purkis, S.J.; Klemas, V.V. *Remote Sensing and Global Environmental Change*; John Wiley & Sons: Hoboken, NJ, USA, 2011.
19. Kenny, A.J.; Cato, I.; Desprez, M.; Fader, G.; Schüttenhelm, R.T.E.; Side, J. An overview of seabed-mapping technologies in the context of marine habitat classification. *ICES J. Mar. Sci.* **2003**, *60*, 411–418. [[CrossRef](#)]
20. Marcello, J.; Eugenio, F.; Martín, J.; Marqués, F. Seabed mapping in coastal shallow waters using high resolution multispectral and hyperspectral imagery. *Remote Sens.* **2018**, *10*, 1208. [[CrossRef](#)]
21. Veettil, B.K.; Ward, R.D.; Lima, M.D.A.C.; Stankovic, M.; Hoai, P.N.; Quang, N.X. Opportunities for seagrass research derived from remote sensing: A review of current methods. *Ecol. Indic.* **2020**, *117*, 106560. [[CrossRef](#)]
22. Mederos-Barrera, A.; Marcello, J.; Eugenio, F.; Hernández, E. Seagrass mapping using high resolution multispectral satellite imagery: A comparison of water column correction models. *Int. J. Appl. Earth Obs. Geoinf.* **2022**, *113*, 102990. [[CrossRef](#)]
23. Eugenio, F.; Marcello, J.; Mederos-Barrera, A.; Marqués, F. High Resolution Satellite Bathymetry Mapping: Regression and Machine Learning Based Approaches. *IEEE Trans. Geosci. Remote Sens.* **2022**, *60*, 5407614. [[CrossRef](#)]
24. Blake, C.; Maggs, C.A. Comparative growth rates and internal banding periodicity of maërl species (*Corallinales*, *Rhodophyta*) from northern Europe. *Phycologia* **2003**, *42*, 606–612. [[CrossRef](#)]
25. Barbera, C.; Bordehore, C.; Borg, J.A.; Glémarec, M.; Grall, J.; Hall-Spencer, J.M.; de la Huz, C.; Lanfranco, E.; Lastra, M.; Moore, P. Conservation and management of northeast Atlantic and Mediterranean maërl beds. *Aquat. Conserv. Mar. Freshw. Ecosyst.* **2003**, *13*, S65–S76. [[CrossRef](#)]
26. Nelson, W.A. Calcified macroalgae—Critical to coastal ecosystems and vulnerable to change: A review. *Mar. Freshw. Res.* **2009**, *60*, 787–801. [[CrossRef](#)]
27. Sathyendranath, S. *Remote Sensing of Ocean Colour in Coastal, and Other Optically-Complex, Waters*; International Ocean Colour Coordinating Group: Dartmouth, NS, Canada, 2000.
28. McFeeters, S.K. The use of the Normalized Difference Water Index (NDWI) in the delineation of open water features. *Int. J. Remote Sens.* **1996**, *17*, 1425–1432. [[CrossRef](#)]
29. Updike, T.; Comp, C. *Radiometric Use of WorldView-2 Imagery*; Technical Note; DigitalGlobe: Westminster, CO, USA, 2010; pp. 1–17.
30. Labsch, H.; Handorf, D.; Dethloff, K.; Kurgansky, M.V. Atmospheric circulation regimes in a nonlinear quasi-geostrophic model. *Adv. Meteorol.* **2015**, 629429. [[CrossRef](#)]
31. Eugenio, F.; Marcello, J.; Martin, J. High-Resolution Maps of Bathymetry and Benthic Habitats in Shallow-Water Environments Using Multispectral Remote Sensing Imagery. *IEEE Trans. Geosci. Remote Sens.* **2015**, *53*, 3539–3549. [[CrossRef](#)]
32. Eugenio, F.; Marcello, J.; Martin, J.; Rodríguez-Esparragón, D. Benthic Habitat Mapping Using Multispectral High-Resolution Imagery: Evaluation of Shallow Water Atmospheric Correction Techniques. *Sensors* **2017**, *17*, 2639. [[CrossRef](#)]
33. Vermote, E.F.T.D.; Tanré, D.; Deuzé, J.L.; Herman, M.; Morcrette, J.J.; Kotchenova, S.Y. *Second Simulation of a Satellite Signal in the Solar Spectrum-Vector (6SV)*; 6S User Guide Version; University of Maryland: Maryland, DC, USA, 2006; Volume 3, pp. 1–55.
34. Kay, S.; Hedley, J.D.; Lavender, S. Sun glint correction of high and low spatial resolution images of aquatic scenes: A review of methods for visible and near-infrared wavelengths. *Remote Sens.* **2009**, *1*, 697–730. [[CrossRef](#)]

35. Lyzenga, D.R.; Malinas, N.P.; Tanis, F.J. Multispectral bathymetry using a simple physically based algorithm. *IEEE Trans. Geosci. Remote Sens.* **2006**, *44*, 2251–2259. [[CrossRef](#)]
36. Hedley, J.D.; Harborne, A.R.; Mumby, P.J. Simple and robust removal of sun glint for mapping shallow-water benthos. *Int. J. Remote Sens.* **2005**, *26*, 2107–2112. [[CrossRef](#)]
37. Salehi, B.; Zhang, Y.; Zhong, M. Automatic moving vehicles information extraction from single-pass WorldView-2 imagery. *IEEE J. Sel. Top. Appl. Earth Obs. Remote Sens.* **2012**, *5*, 135–145. [[CrossRef](#)]
38. Coffey, M.M.; Whitman, P.J.; Schaeffer, B.A.; Hill, V.; Zimmerman, R.C.; Salls, W.B.; Graybill, D.D. Vertical artifacts in high-resolution WorldView-2 and WorldView-3 satellite imagery of aquatic systems. *Int. J. Remote Sens.* **2022**, *43*, 1199–1225. [[CrossRef](#)] [[PubMed](#)]
39. Mather, P.; Tso, B. *Classification Methods for Remotely Sensed Data*; CRC Press: Boca Raton, FL, USA, 2016.
40. Sheykhou, M.; Mahdianpari, M.; Ghanbari, H.; Mohammadimanesh, F.; Ghamisi, P.; Homayouni, S. Support vector machine versus random forest for remote sensing image classification: A meta-analysis and systematic review. *IEEE J. Sel. Top. Appl. Earth Obs. Remote Sens.* **2020**, *13*, 6308–6325. [[CrossRef](#)]
41. Chirici, G.; Mura, M.; McInerney, D.; Py, N.; Tomppo, E.O.; Waser, L.T.; Travaglini, D.; McRoberts, R.E. A meta-analysis and review of the literature on the k-Nearest Neighbors technique for forestry applications that use remotely sensed data. *Remote Sens. Environ.* **2016**, *176*, 282–294. [[CrossRef](#)]
42. Maulik, U.; Chakraborty, D. Remote Sensing Image Classification: A survey of support-vector-machine-based advanced techniques. *IEEE Geosci. Remote Sens. Mag.* **2017**, *5*, 33–52. [[CrossRef](#)]
43. Zhu, X.X.; Tuia, D.; Mou, L.; Xia, G.S.; Zhang, L.; Xu, F.; Fraundorfer, F. Deep learning in remote sensing: A comprehensive review and list of resources. *IEEE Geosci. Remote Sens. Mag.* **2017**, *5*, 8–36. [[CrossRef](#)]
44. Yuan, Q.; Shen, H.; Li, T.; Li, Z.; Li, S.; Jiang, Y.; Xu, H.; Tan, W.; Yang, Q.; Wang, J.; et al. Deep learning in environmental remote sensing: Achievements and challenges. *Remote Sens. Environ.* **2020**, *241*, 111716. [[CrossRef](#)]
45. Rukundo, O.; Cao, H. Nearest neighbor value interpolation. *Int. J. Adv. Comput. Sci. Appl.* **2012**, *3*, 4.
46. Martin, S.; Clavier, J.; Chauvaud, L.; Thouzeau, G. Community metabolism in temperate maerl beds. I. Carbon and carbonate fluxes. *Mar. Ecol. Prog. Ser.* **2007**, *335*, 19–29. [[CrossRef](#)]
47. Ceccherelli, G.; Cinelli, F. Short-term effects of nutrient enrichment of the sediment and interactions between the seagrass *Cymodocea nodosa* and the introduced green alga *Caulerpa taxifolia* in the Mediterranean bay. *J. Exp. Mar. Biol. Ecol.* **1997**, *217*, 165–177. [[CrossRef](#)]
48. Ceccherelli, G.; Sechi, N. Nutrient availability in the sediment and the reciprocal effects between the native seagrass *Cymodocea nodosa* and the introduced rhizophytic alga *Caulerpa taxifolia*. *Hydrobiologia* **2002**, *474*, 57–66. [[CrossRef](#)]
49. Stumpf, R.P.; Holderied, K.; Sinclair, M. Determination of water depth with high-resolution satellite imagery over variable bottom types. *Limnol. Oceanogr.* **2003**, *48*, 547–556. [[CrossRef](#)]
50. Gobierno de Canarias. *Censo De Vertidos Desde Tierra Al Mar En Canarias: Emisario Submarino de La Batata—Ensenada Pelada (Code 02TFGR, ID 416)*; Gobierno de Canarias: Las Palmas de Gran Canaria, Spain, 2021. Available online: https://www.idecanarias.es/recursos/Vertidos_2021/Fichas/Tenerife/416.pdf (accessed on 6 March 2022).
51. Grupo Tragsa. *Actualización del Censo de Vertidos Desde Tierra al mar en Canarias 2021: Memoria General Canarias*; Gobierno de Canarias: Las Palmas de Gran Canaria, Spain, 2022. Available online: https://www.gobiernodecanarias.org/medioambiente/descargas/Aguas/Censo_vertidos_2021/01-MEMORIAS/Canarias.pdf (accessed on 6 March 2022).
52. Pérez-Fernández, J. *Contribución al Conocimiento del Efecto de Los Emisarios Submarinos y Los Diques Sobre Las Praderas Marinas de "Cymodocea Nodosa": Estudio del Emisario Submarino de la Playa de El Cochino y el Dique Del Puerto de Taliarte en Gran Canaria*; Universidad de Las Palmas de Gran Canaria: Las Palmas de Gran Canaria, Spain, 2001.

Disclaimer/Publisher's Note: The statements, opinions and data contained in all publications are solely those of the individual author(s) and contributor(s) and not of MDPI and/or the editor(s). MDPI and/or the editor(s) disclaim responsibility for any injury to people or property resulting from any ideas, methods, instructions or products referred to in the content.